

Supporting Information for Ligand Effects in Assembly of Cubic and Spherical Nanocrystals: Applications to Packing of Perovskite Nanocubes.

Jonas Hallstrom,^{*,†} Ihor Cherniukh,[‡] Xun Zha,[†] Maksym V. Kovalenko,[‡] and
Alex Travesset^{*,†}

[†]*Department of Physics and Astronomy, Iowa State University and Ames National
Laboratory, Ames, IA 50011, USA*

[‡]*Institute of Inorganic Chemistry, Department of Chemistry and Applied Biosciences, ETH
Zurich, CH-8093 Zurich, Switzerland; Laboratory for Thin Films and Photovoltaics,
Empa-Swiss Federal Laboratories for Materials Science and Technology, CH-8600,
Dübendorf, Switzerland.*

E-mail: jllhallst@asu.edu; trvsst@ameslab.gov

Force Field Parameters

To graft each DDAB ligand, the N^+ ion of the ligand was placed a distance of 0.255 nm from a Br^- ion of the core. The N^+ ions are modeled as rigid bodies along with the cores, keeping this distance constant throughout simulation.

New force field parameters are listed in Tables S1, S2, S3, and S4.

Table S1: Lennard-Jones 12-6 potential parameters

	ϵ (kJ/mol)	σ (Å)
CH2	0.466	3.96
CH3	0.898	3.76
N	0.711	3.20
Cs	0.795	3.74
Br	0.628	4.04

Table S2: OPLS Bond Parameters

	K_r (kJ/nm ²)	r_0 (Å)
N-CH2	307,106	1.47
N-CH3	307,106	1.47

Table S3: OPLS Angle Parameters

	K_θ (kJ/mol/rad ²)	θ_0 (rad)
CH3-N-CH3	669	1.91
CH2-N-CH2	669	1.91
CH3-N-CH2	669	1.91
N-CH2-CH2	669	1.94

Table S4: OPLS Dihedral Parameters

	V_1 (kJ/mol)	V_2 (kJ/mol)	V_3 (kJ/mol)	V_4 (kJ/mol)
N-CH2-CH2-CH2	5.77	-2.67	0.958	-4.06
CH3-N-CH2-CH2	0.001	0.001	0.001	0.001
CH2-N-CH2-CH2	0.001	0.001	0.001	0.001

Computational Details

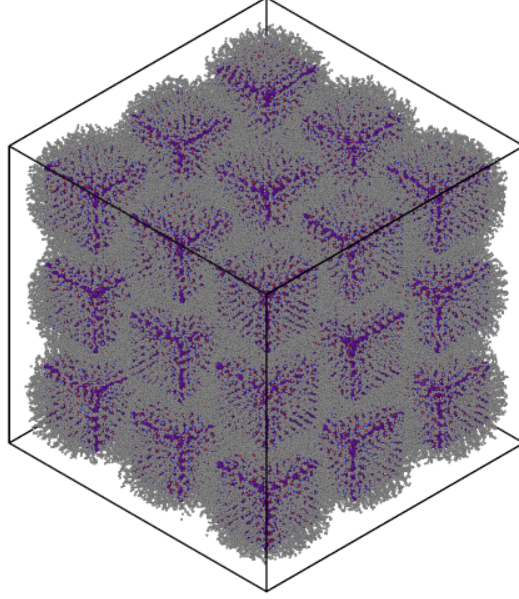


Figure S1: A snapshot of a 3x3x3 simple cubic NCSL made up of $n_{WS} = 7$ ($l_P = 4.11$ nm) and $\sigma = 2.90$ chains/nm² PNCs.

The PMF simulations took about of the order of 10^7 to 10^6 timesteps per window, with different values depending on size, for a total simulated times of 8-46 ns,

Single component simple cubic NCSLs contain $3 \times 3 \times 3$ unit cells, for a total of = 27 NCs, as shown in Fig. S1. The systems are equilibrated for 10^6 time steps (~ 2 ns), and then data is collected from an additional $5 \cdot 10^6$ times steps (~ 10 ns).

To calculate the free energy, simulations are performed with different NC separations, to maintain the lattice space group, nearest neighbors and some next to nearest neighbors are connected by harmonic bonds. The virial tensor is obtained from the simulation and interpolated for further integration to obtain the free energy, as described in Eq. S1.

Virial data is collected every 10^4 time steps, to avoid data relativity for standard error calculation. 100 snapshots are collected to calculate pressure contribution from harmonic springs between NCs; 2 lattices with large NC separation are simulated to calculate the pressure contribution from NC self-interactions; these two extra contributions are subtracted

from the pressure, as shown in Eq. S1. Then the pressure is interpolated and integrated over volume. To precisely locate the minimum free energy, the scipy PchipInterpolator package is used for the interpolation and integration. Minimum free energy of the binary system is compared with that of the type A and type B single-component fcc systems to obtain the minimum free energy difference.

Data of internal energy is also collected and interpolated at the NC separation where the free energy is at minimum, then the internal energy and entropy difference between binary and fcc systems is obtained.

Free Energy Calculations

We placed single component and binary NC systems into pre-defined superlattices according to Ref.,¹ initially at a very large lattice constant and stabilized by harmonic springs. The spherical NC is described by the notation N_d^{lig} , where d =NC core diameter and lig the corresponding ligand. The corresponding BNSL will be denoted as $P_{l_E} - N_d^{lig}$, where l_E has been defined in Eq. 1. The spherical NC cores are built as described in our previous publication.² The free energy of the BNSL is computed by integrating the pressure

$$F_N(T, V) - F_N(T, V_0) = - \int_{a_0}^{a_L} \left(\frac{3Nk_B T}{a_L} + \frac{1}{a_L} \delta^{\alpha\beta} \Pi_{\alpha\beta}(a_L) - \frac{2}{a_L} \langle W \rangle \right) da_L \quad (S1)$$

where a_L is the lattice constant, $\Pi_{\alpha\beta}$ is the virial (pressure) tensor and $\langle W \rangle$ is the average energy of harmonic springs connecting NCs. NVT simulations are performed at multiple values of a_L , starting at a large enough lattice constant a_0 where NC are non-interacting, thus defining the reference state $NV_0(a_0)T$. The NC are modeled as rigid bodies and are prevented from rotation by not integrating the rotational degrees of freedom. Only one temperature $T = T_m$, where $T_m = 387$ K has been considered. All simulations are done in vacuum, in the absence of solvent, thus, the final state is the same as in an experiment where all solvent has been evaporated, *i.e.* a dry sample. We define the zero free energy as

the reference state, *i.e.* the superlattice at an infinitely large lattice constant.

Relevant Observables

We will follow the notation that d^{sim}, l_E^{sim} are the diameters obtained from the minimum of the single component (fcc/bcc or sc) free energy, where we follow the convention that B(blue) is the PNC and A(red) the spherical NC. Then d^{HS}, l^{HS} are the HS diameter of each NC computed according to OPM, with γ given by EqYYY. In the presence of OTM branches, the effective diameters may differ from HS, which we will denote as \bar{d}_A, \bar{d}_B and their ratio according to $\bar{\gamma}$. Here $\bar{d}_A^{sim}, \bar{d}_B^{sim}$ and $\bar{\gamma}_{sim}$ are the same quantities, as obtained from the minimum of the free energy in the simulations.

The free energy of any superlattice is computed from Eq. S1. In addition, the internal energy U is computed directly from the simulation and the entropy from $S = (U - F)/T$.

Measure of Interdigitation

We quantify the degree of interdigitation by counting how many "offsider" ligand particles there are in each Face-Face PMF with an offsider particle defined as belonging to Nanoparticle 1 but being closer to Nanoparticle 2, or vice versa. The graph of the average number of offsider ligand particles for a configuration at equilibrium (at a nanoparticle separation that minimizes free energy) is given in Fig. S2.

As shown in Fig. S2, there is a clear correlation between the value of the free energy and the degree of interdigitation. The number of offsider particles is graphed in the negative axis to highlight the similar trends in the two graphs.

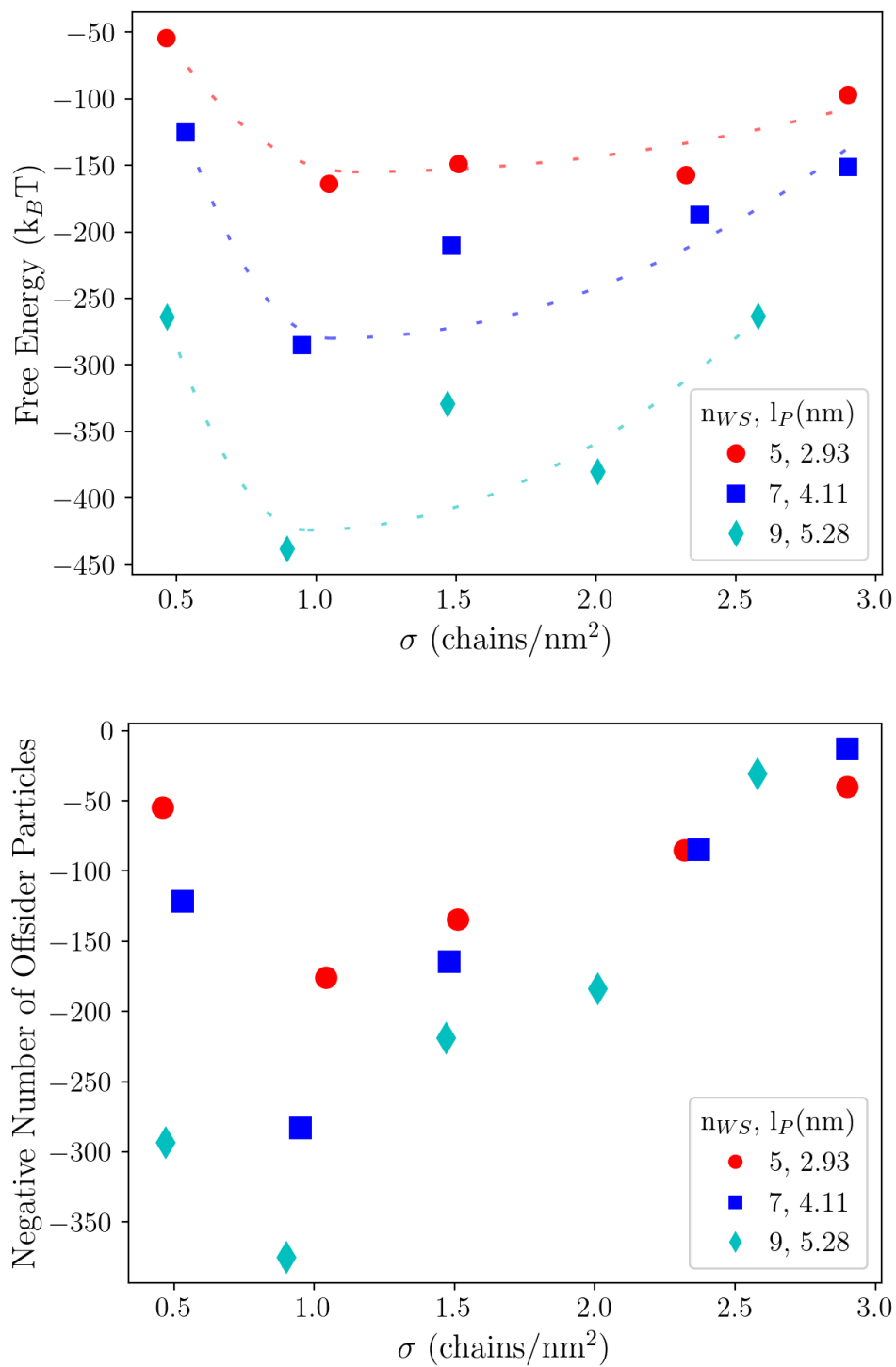


Figure S2: (Top) Minimum free energy and (bottom) degree of interdigitation as functions of nanoparticle grafting density and size.

Experimental Details

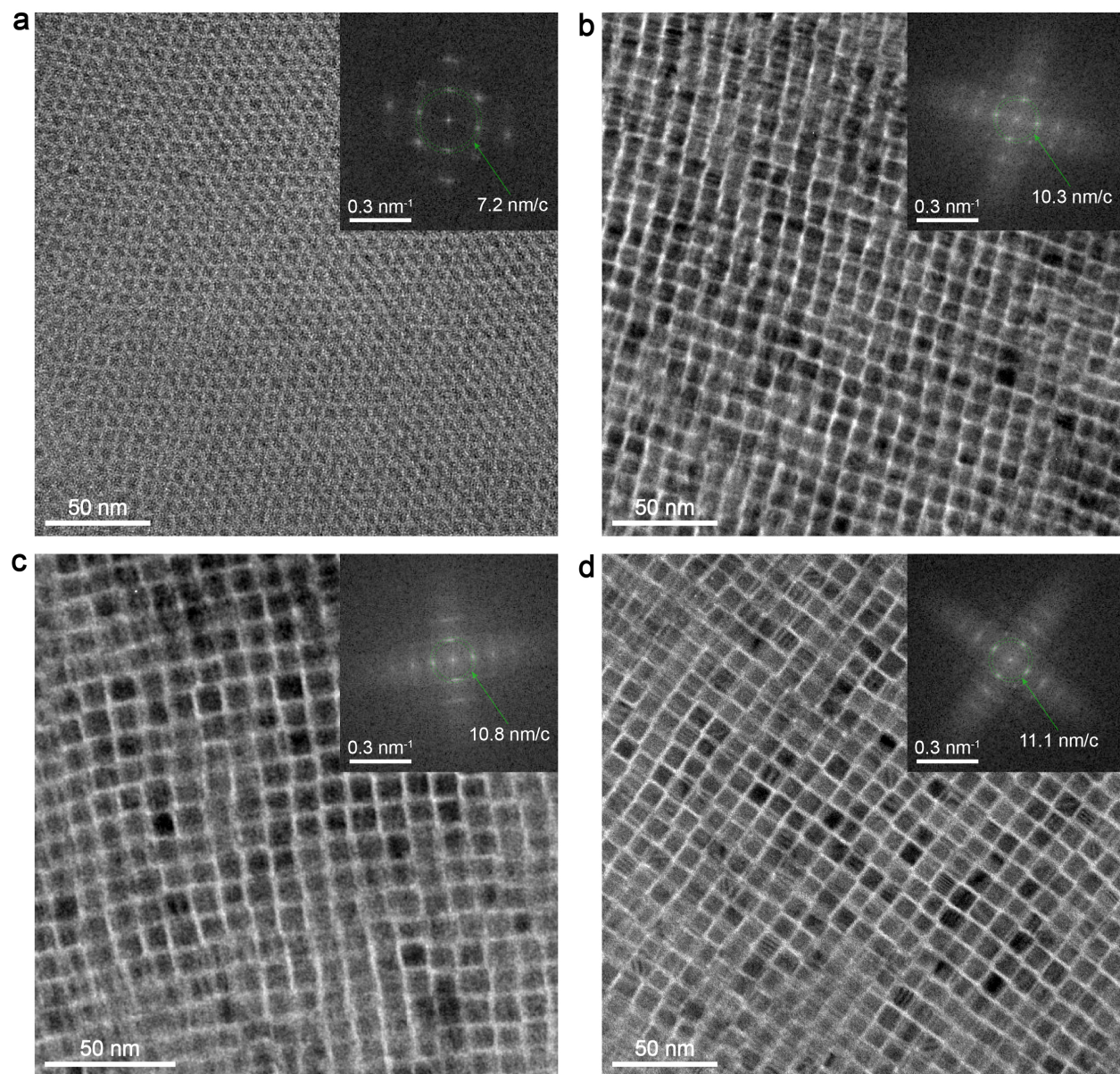


Figure S3: TEM images and corresponding FFT patterns of the superlattices obtained from (a) 5.6 nm, (b) 8.8 nm, (c) 9.3 nm, (d) 9.8 nm CsPbBr₃ NCs.

CsPbBr₃ NCs. 9.8 nm NCs were synthesized following the method reported in Ref.³ In a 25 mL three-neck flask, PbBr₂ (55 mg, ABCR, 98%) was degassed three times, suspended in 5 mL 1-octadecene (ODE, Sigma-Aldrich, 90%, distilled), degassed three times again at room temperature. The suspension was fast heated up to 190 C, when the temperature reached 125

C, 0.5 mL oleic acid (OA, Sigma-Aldrich, 90%, vacuum-dried at 100 C) and oleylamine (0.5 mL, OLA, Strem, 97%, distilled) were injected. At 190 C, pre-heated to about 100 C cesium oleate solution in ODE [0.6 mL, prepared by reacting 0.2 g Cs₂CO₃ (Sigma-Aldrich, 99.9%), 0.6 mL OA and 7.5 mL ODE at 120 C for 20 min under vacuum] was injected. The reaction mixture was cooled immediately to room temperature with an ice bath. The crude solution was centrifuged at 12100 revolutions per minute (rpm, equivalent to 20130 relative centrifugal force) for 5 min, the supernatant was discarded and the precipitate was dispersed in hexane (0.3 mL, Sigma-Aldrich, anhydrous, 95%). The solution was centrifuged again at 10000 rpm for 3 min and the precipitate was discarded. Then, OLA/OA ligands were exchanged by Didodecyldimethylammonium bromide (DDAB, Sigma-Aldrich, 98%) treatment. 0.3 mL hexane, toluene (0.6 mL, Sigma-Aldrich, anhydrous, 99.8%), and DDAB/PbBr₂ solution (0.14 mL, 0.066 M DDAB and 0.033 M PbBr₂ in toluene) were added to the supernatant and stirred for 1h, followed by destabilization with ethyl acetate (1.8 mL, Sigma-Aldrich, 99.9%), centrifuging at 12100 rpm for 3 min and re-dispersion in 1 mL toluene. Synthesis of 9.3 and 8.8 nm NCs was performed with decreased to 180 and 173 C, respectively, injection temperature. Synthesis of 5.3 nm CsPbBr₃ NCs was adopted from Ref.s^{4,5} followed by DDAB treatment.

Preparation of superlattices and estimation of lattice constants proceeded by self-assembly of NCs by drying ca. 0.8 μ M solution of NCs in toluene over carbon-coated transmission electron microscopy (TEM) grids (carbon type B, Ted Pella, Formvar protective layer was removed by immersing the grid in toluene for 10 s) in a tilted 2 mL glass vial under 0.5 atm pressure at room temperature. Lattice constants were derived from TEM images (collected with the use of JEOL JEM2200FS microscope operating at 200 kV accelerating voltage) and the corresponding FFT patterns using an open-source software Fiji.

Additional Comments on the Hard Shape of PNCs

The actual number of ligands in the PNC is given by $n_{lig} = \sigma l_P^2$. If the number n_{lig} is used, it is assumed that the SC achieves a packing fraction $\eta = 1$. This is not possible, because the linkers are not flexible enough to achieve this perfect packing. This limitation on the ligand is included In Eq. 2 by replacing $n_{lig} = \sigma l_P^2$ by the effective number $n_{lig}^* \sigma l_E^2$ instead, by assuming that $\eta = 1$ might be achieved if the linker was assumed as part of the core and additional dodecyl chains were added.

In Fig. S4 it is shown that the lattice constant of the SC lattice agrees very accurately with the HS edge as obtained from the PMF. The lattice constant in Ref.⁶ used the formula

$$l_{HS} = l_p + 2\xi L \quad (S2)$$

with $\sigma_{Max} = 2.3$, which is Eq. 5 with $l_k = 0$. In Fig. S4 it is shown that at the experimental grafting density $\sigma \approx 0.8$, there is reasonable agreement with the actual formula presented here, Eq. 3.

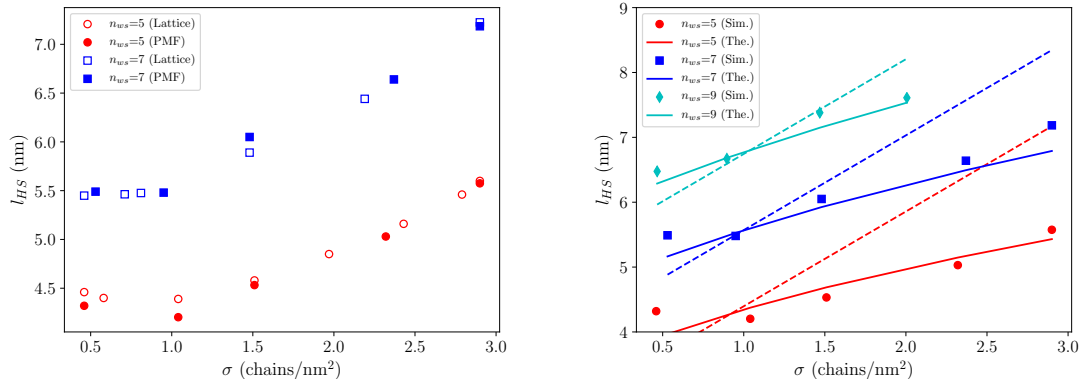


Figure S4: (Left) Comparison between the minima of the PMF and the minimum lattice constant of the SC superlattice. (Right) Same plot as in Fig. 4 including the approximate formula Eq. S2.

Illustration of forcefield problems

Fig. S5 shows four still snapshots of the time sequence leading to united atom overlaps. For clarity, the other ligands and atoms have been removed. The final snapshot shows a CH_2 united atom squeezed inside a gold and sulphur atom, in what is clearly an unphysical configuration. A movie is provided also.

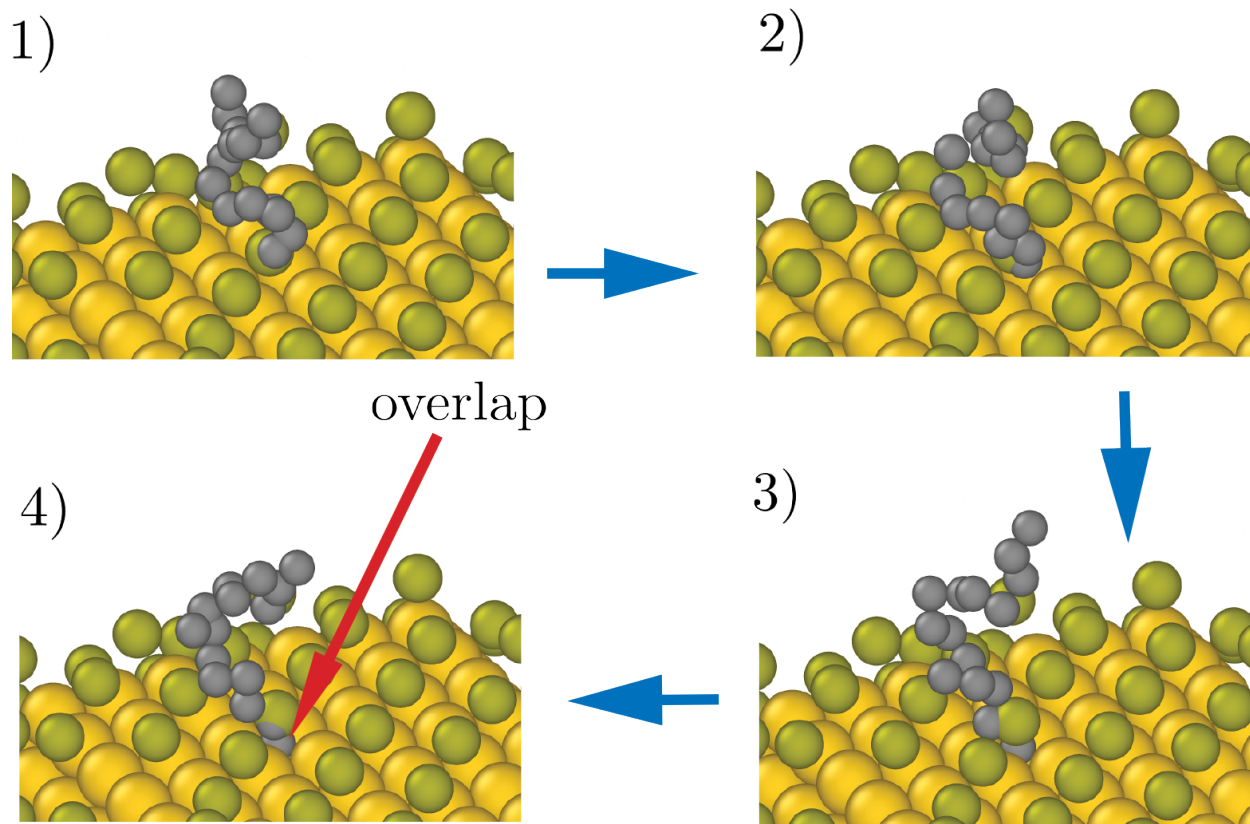


Figure S5: Overlap as a problem for the force field.

Potential of Mean Force

The reproducibility of the PMF was ensured by repeating it with different additional initial conditions, and also by computing it by both WHAM and by integrating the force on the NC to obtain the reversible work, in all cases, the agreement was within $3k_B T$ s. Large fluctuations in the internal energy are apparent in the figures below. This is a result that has been reported previously,⁷ but does not affect the free energy, as the internal energy is computed by averaging the instantaneous internal energy. A more detailed study of this point is beyond the scope of this paper and will be presented elsewhere.

Table S5: Minimum of PMF for Face-Face Configurations

Cube n_{WS} , l_P (nm)	Cube σ (chains/nm ²)	r_{min} (nm)	F_{min} (k _B T)
5, 2.93	0.46	4.33	-54.2
5, 2.93	1.04	4.21	-164
5, 2.93	1.51	4.53	-149
5, 2.93	2.32	5.03	-157
5, 2.93	2.90	5.59	-97
7, 4.11	0.53	5.50	-125
7, 4.11	0.95	5.49	-285
7, 4.11	1.48	6.10	-210
7, 4.11	2.37	6.65	-187
7, 4.11	2.90	7.19	-151
9, 5.28	0.47	6.49	-264
9, 5.28	0.90	6.67	-438
9, 5.28	1.47	7.39	-329
9, 5.28	2.01	7.61	-380
9, 5.28	2.58	8.27	-263

Table S6: Minimum of PMF for Additional Configurations

Configuration	Cube n_{WS} , l_P (nm)	Cube σ (chains/nm ²)	r_{min} (nm)	F_{min} (k _B T)
Face-Turned Face	5, 2.93	1.04	4.17	-173
Edge-Edge	5, 2.93	1.04	4.73	-100
Edge-Edge	9, 5.28	0.47	8.02	-97
Edge-Edge	9, 5.28	0.90	8.24	-161
Edge-Edge	9, 5.28	1.47	8.26	-212
ABO ₃ Corner-Corner	5, 2.93	1.04	5.36	-59
ABO ₃ Corner-Corner	9, 5.28	0.47	9.42	-34
ABO ₃ Corner-Corner	9, 5.28	0.90	9.36	-53
ABO ₃ Corner-Corner	9, 5.28	1.47	9.37	-71
SC Corner-Corner	5, 2.93	1.04	5.45	-44
SC Corner-Corner	9, 5.28	0.47	9.60	-31
SC Corner-Corner	9, 5.28	0.90	9.54	-46
SC Corner-Corner	9, 5.28	1.47	9.51	-64
Face-Sphere	5, 2.93	1.04	5.75	-168
Edge-Sphere	5, 2.93	1.04	5.88	-145
Corner-Sphere	5, 2.93	1.04	6.01	-144
Sphere-Sphere	-	-	7.21	-243

Face-Face

$$n_{WS} = 5$$

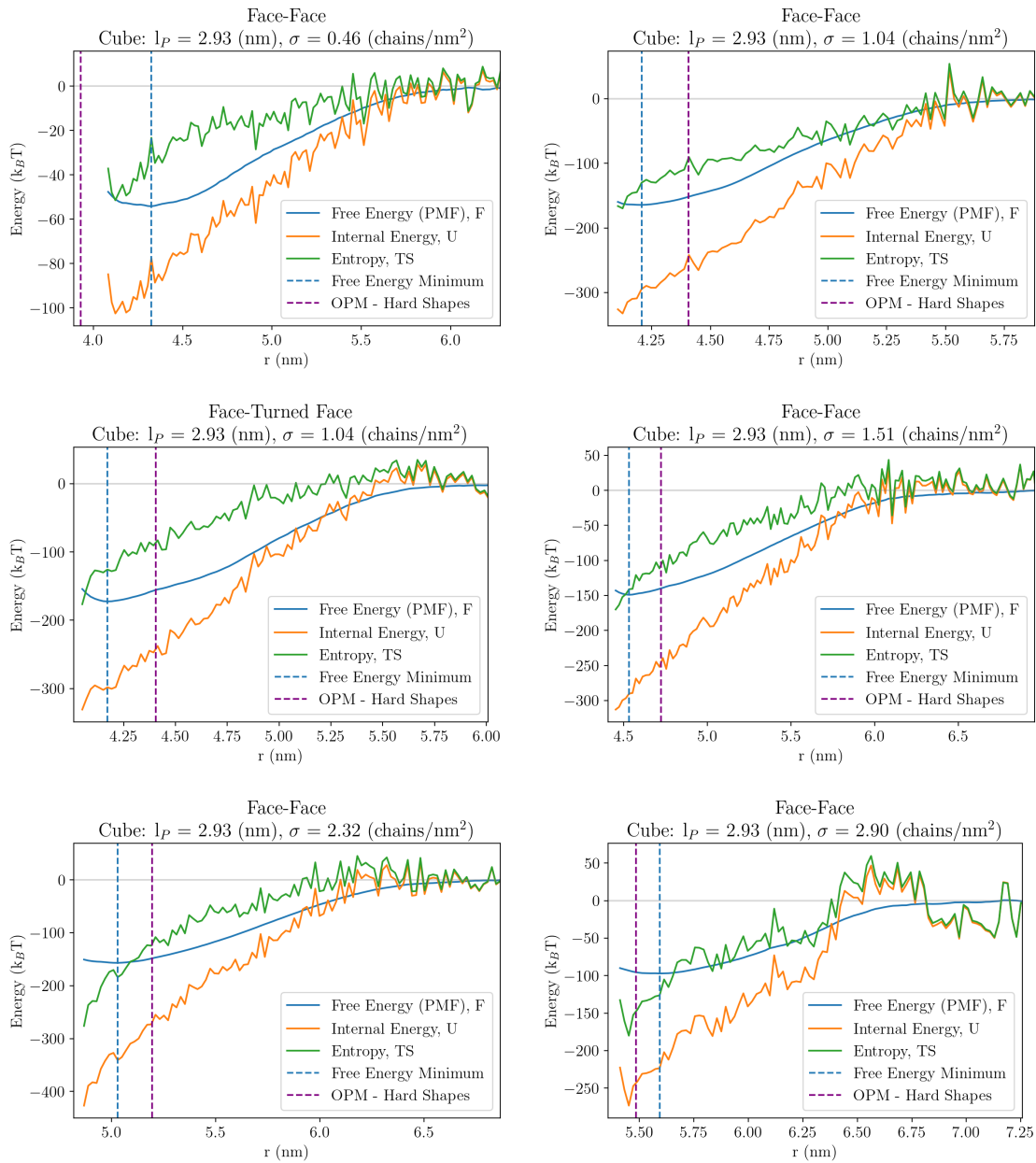


Figure S6: PMFs.

$$n_{WS} = 7$$

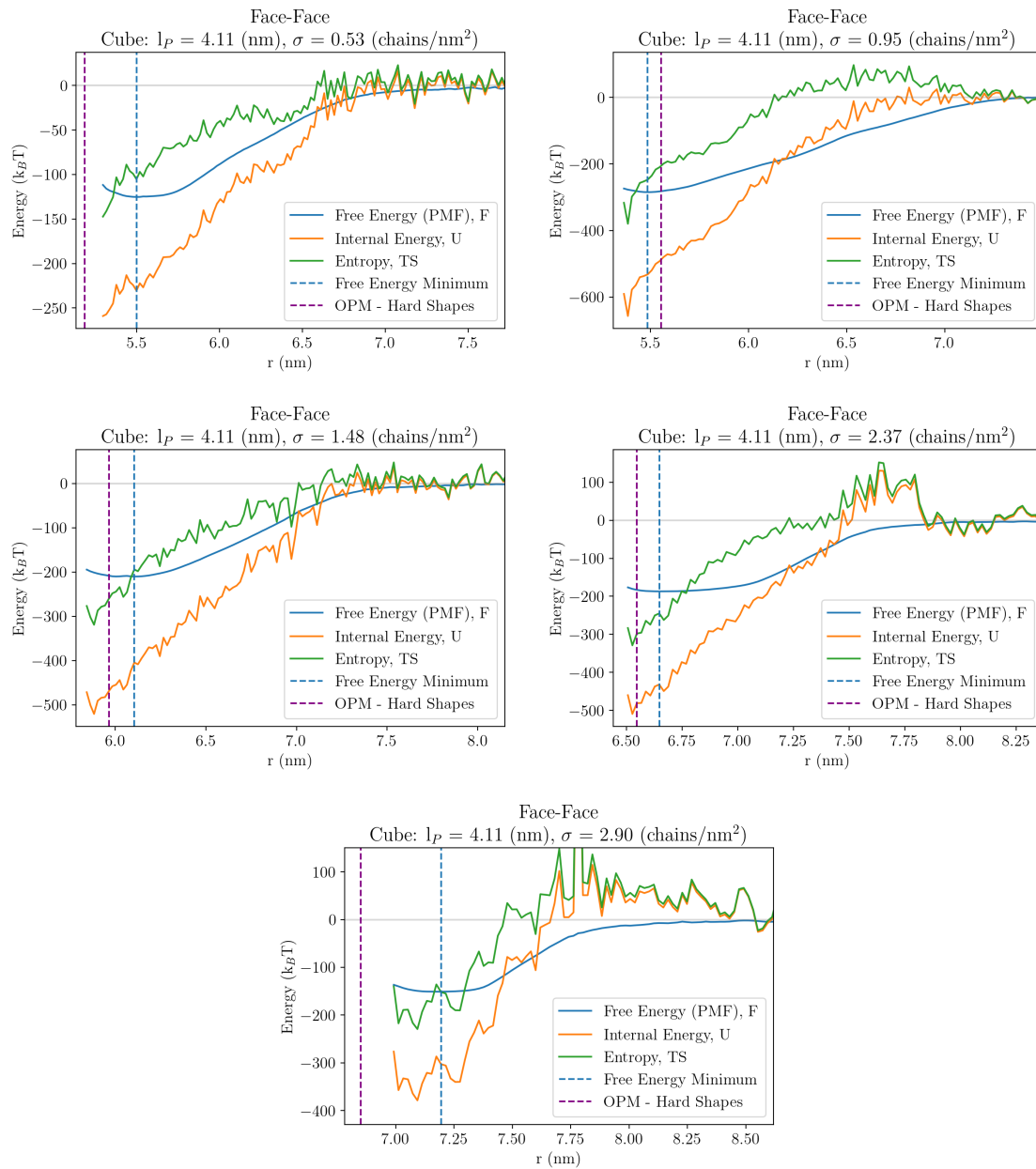


Figure S7: PMFs.

$$n_{WS} = 9$$

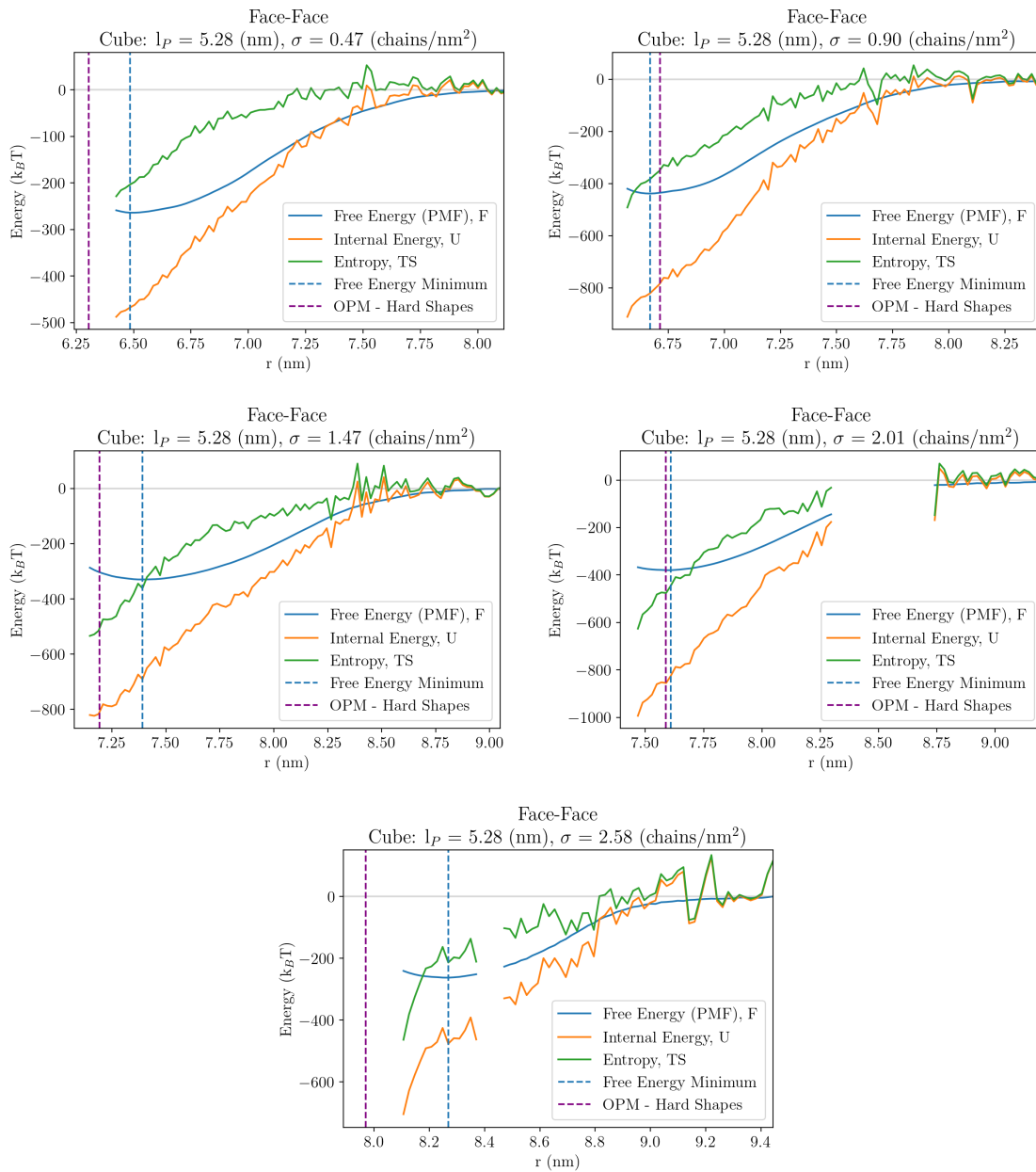


Figure S8: PMFs.

Edge-Edge

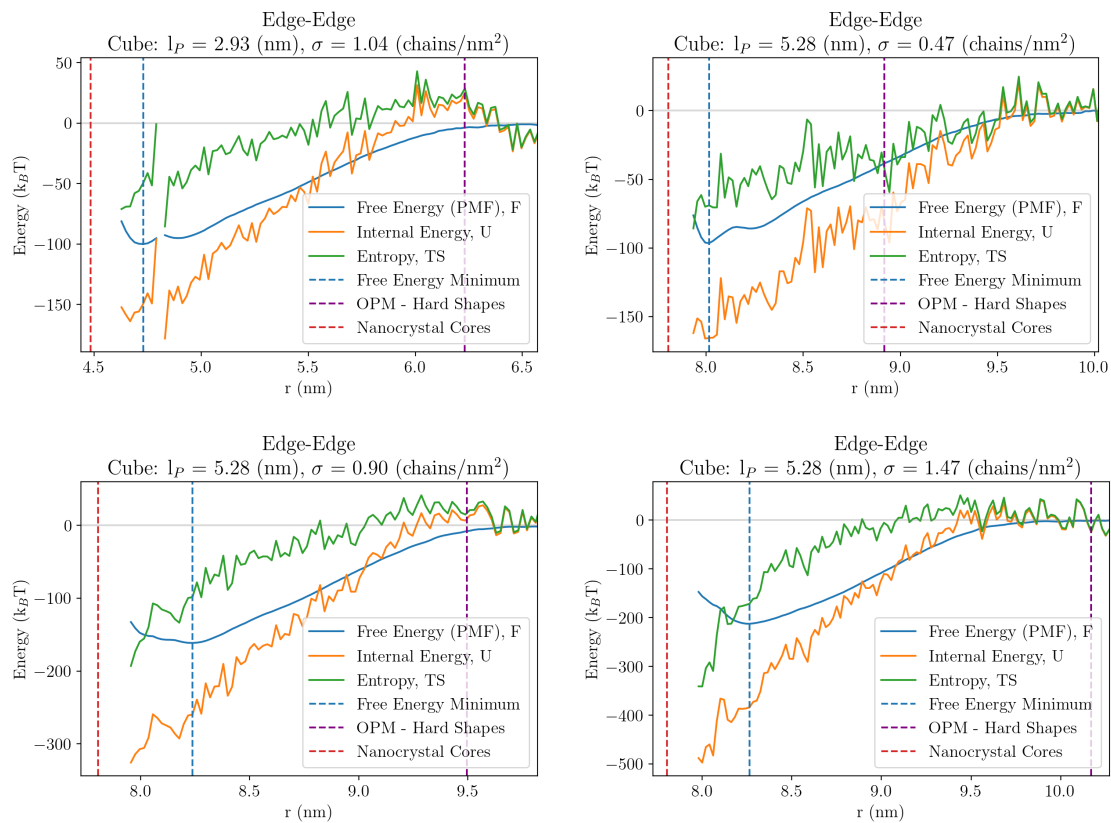


Figure S9: PMFs.

ABO₃ Corner-Corner

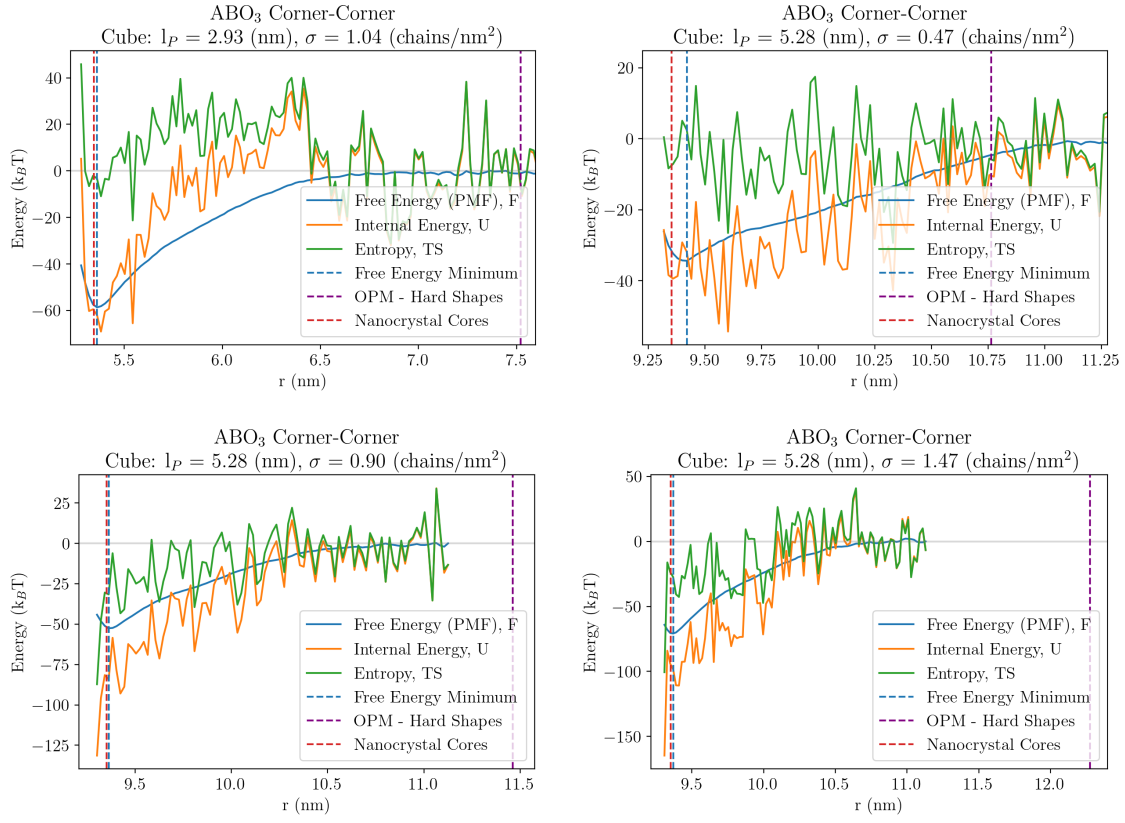


Figure S10: PMFs.

SC Corner-Corner

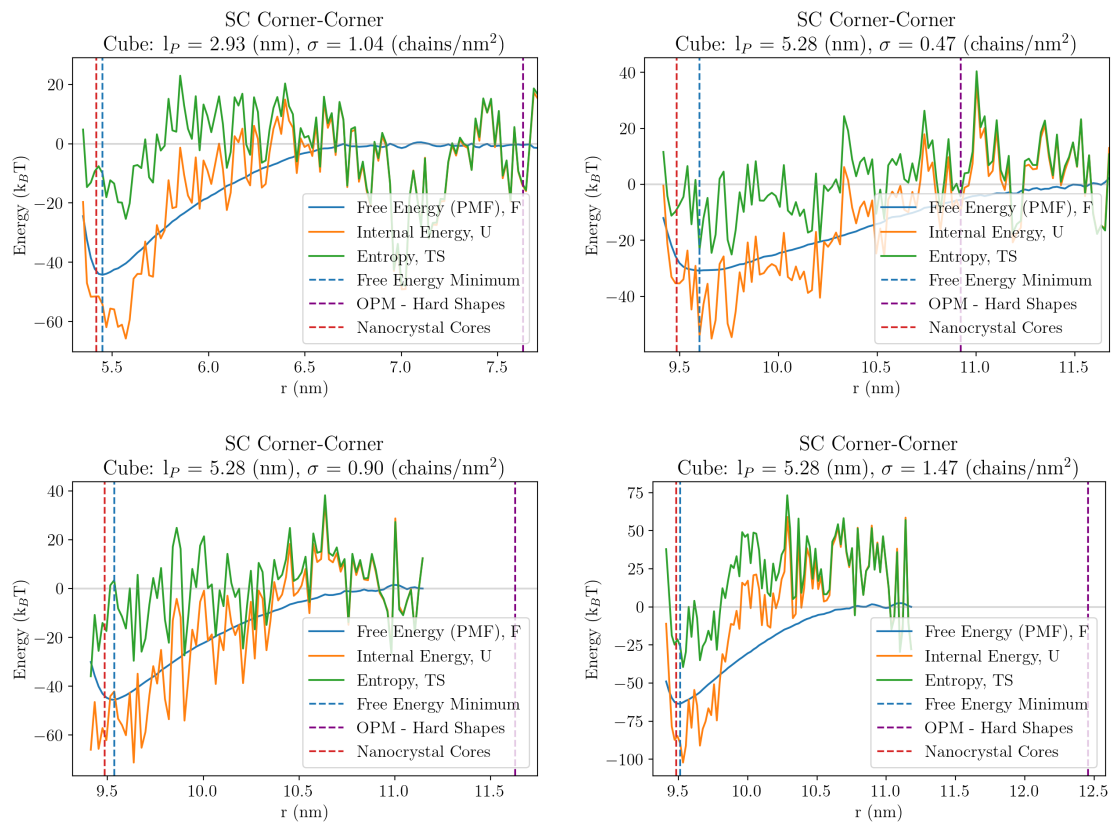


Figure S11: PMFs.

Spheres and Cubes

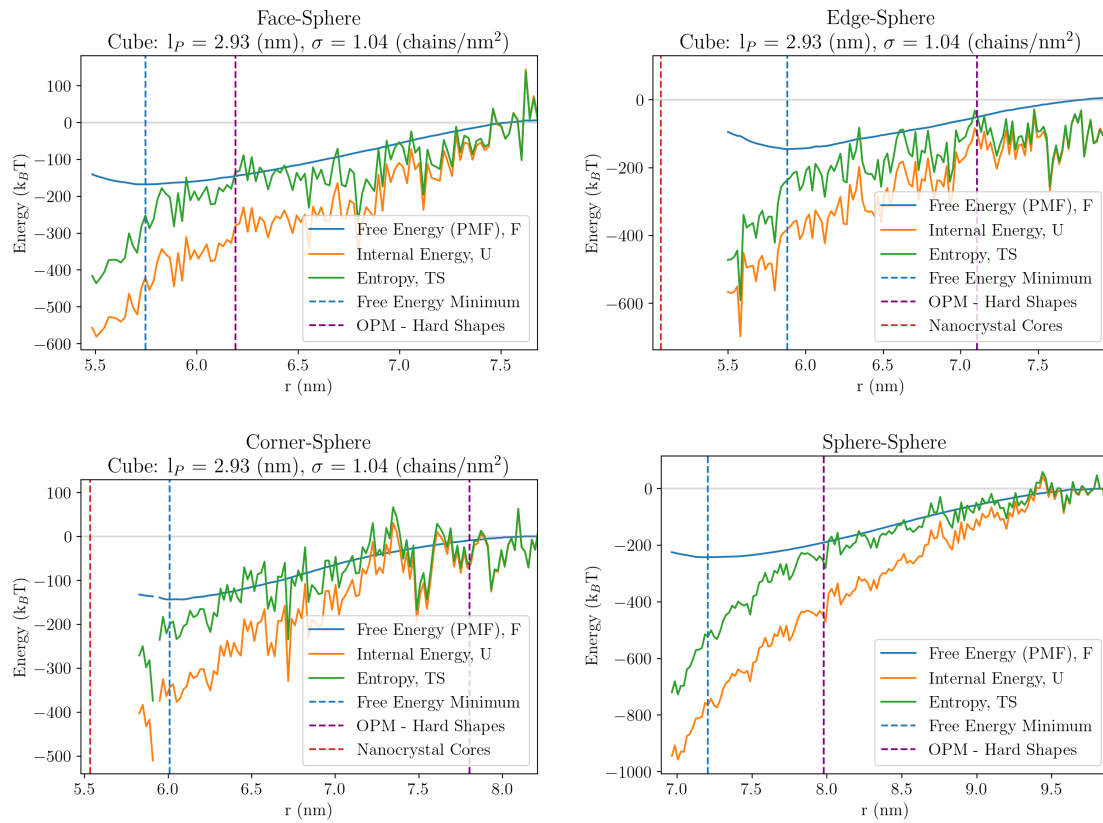


Figure S12: PMFs.

Free Energy of Simple Cubic Superlattices

$$n_{WS} = 5$$

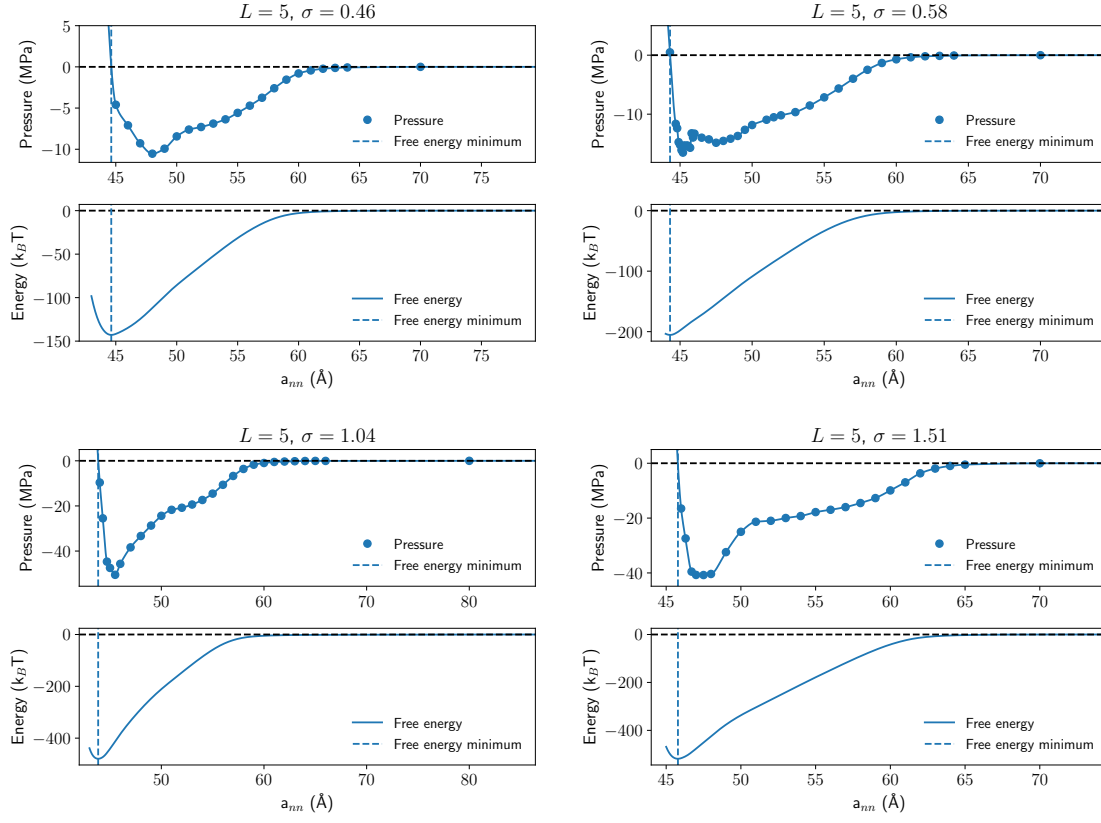


Figure S13: Free energy results of different σ 's for $n_{WS} = 5$.

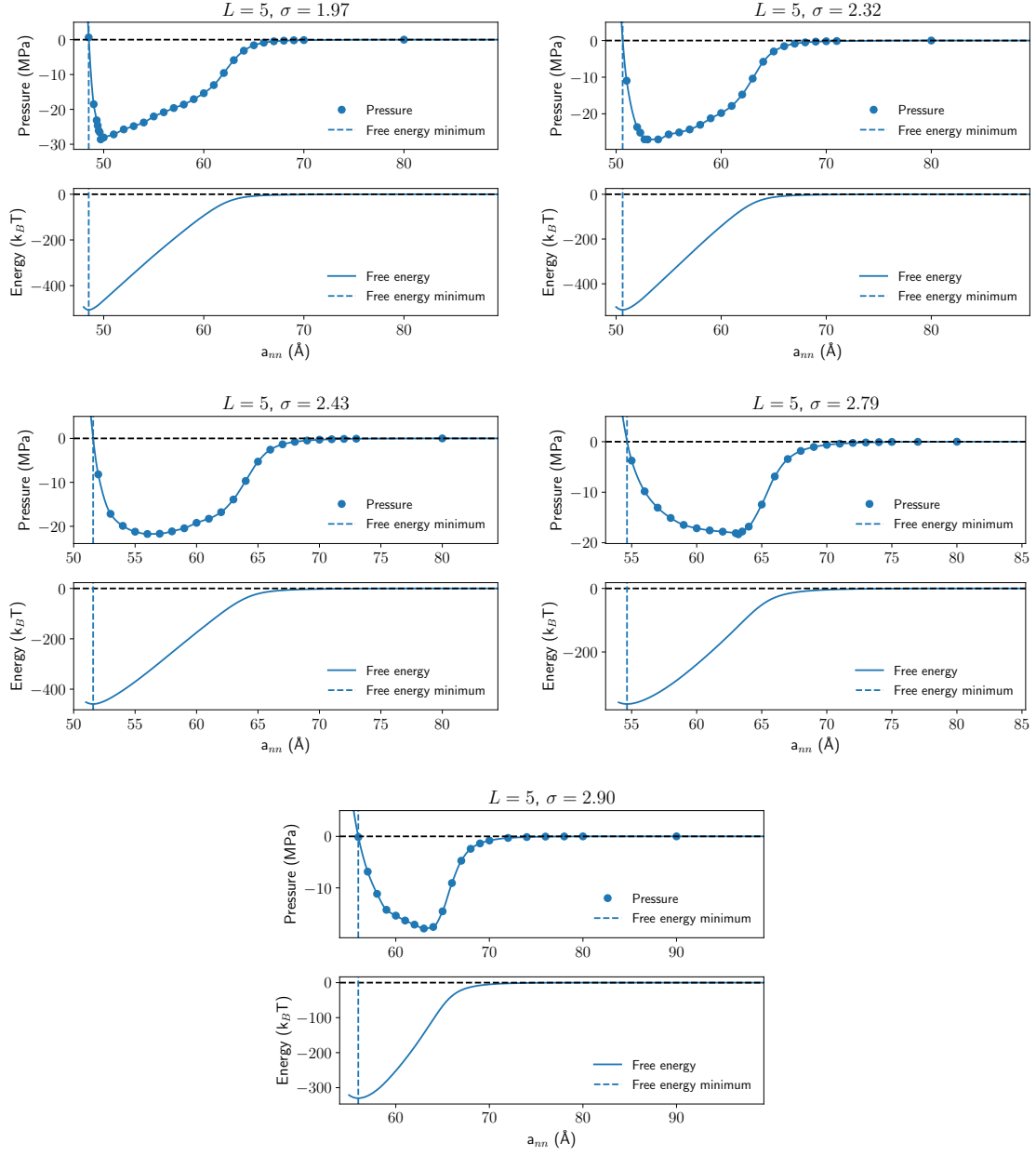


Figure S14: Free energy results of different σ 's for $n_{WS} = 5$.

$$n_{WS} = 7$$

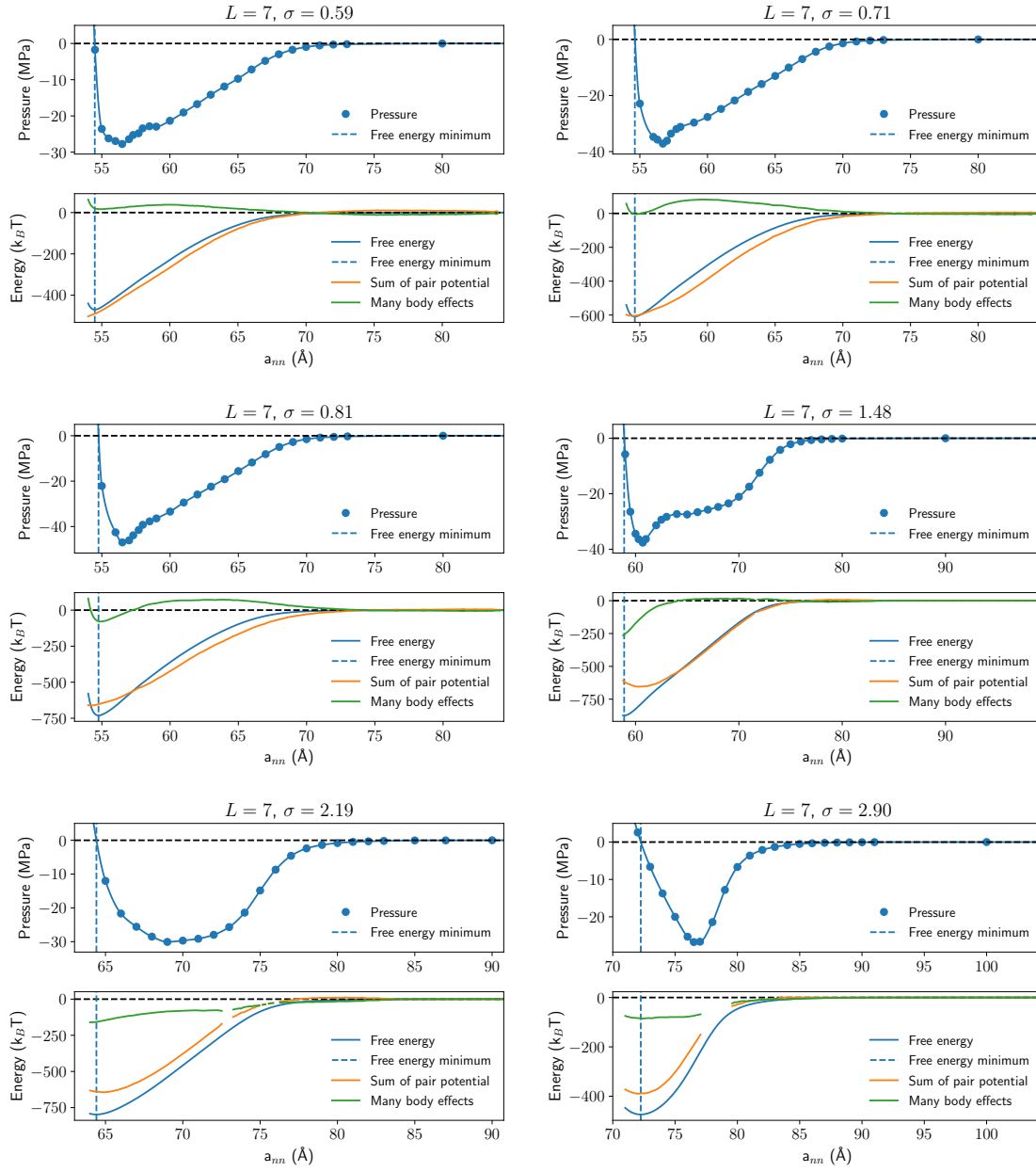


Figure S15: Free energy results of different σ 's for $n_{WS} = 7$.

Equilibrium Snapshots for $n_{WS} = 5$

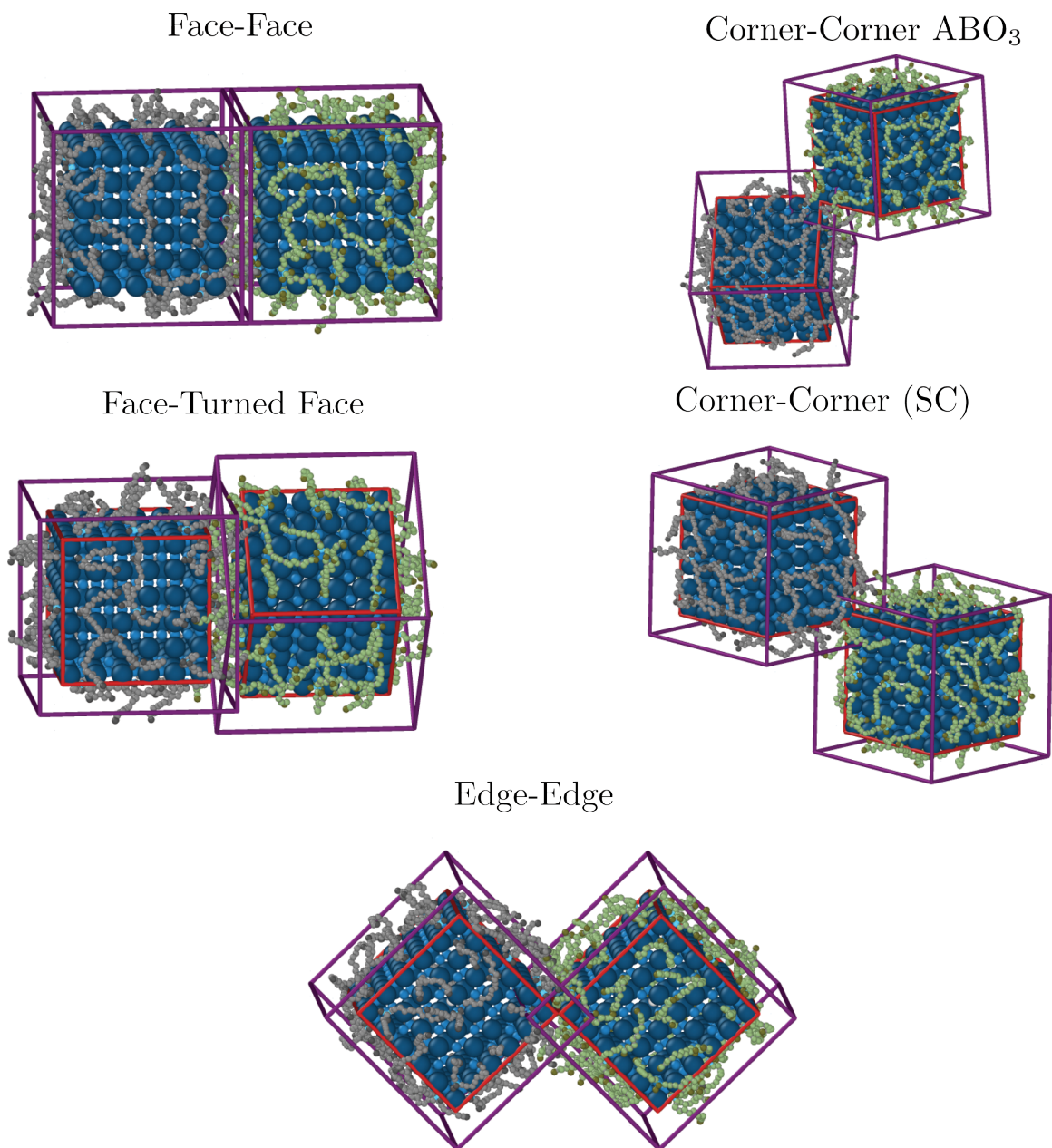


Figure S16: Snapshots for $n_{WS} = 5$.

Additional Illustration of corner-corner vortices

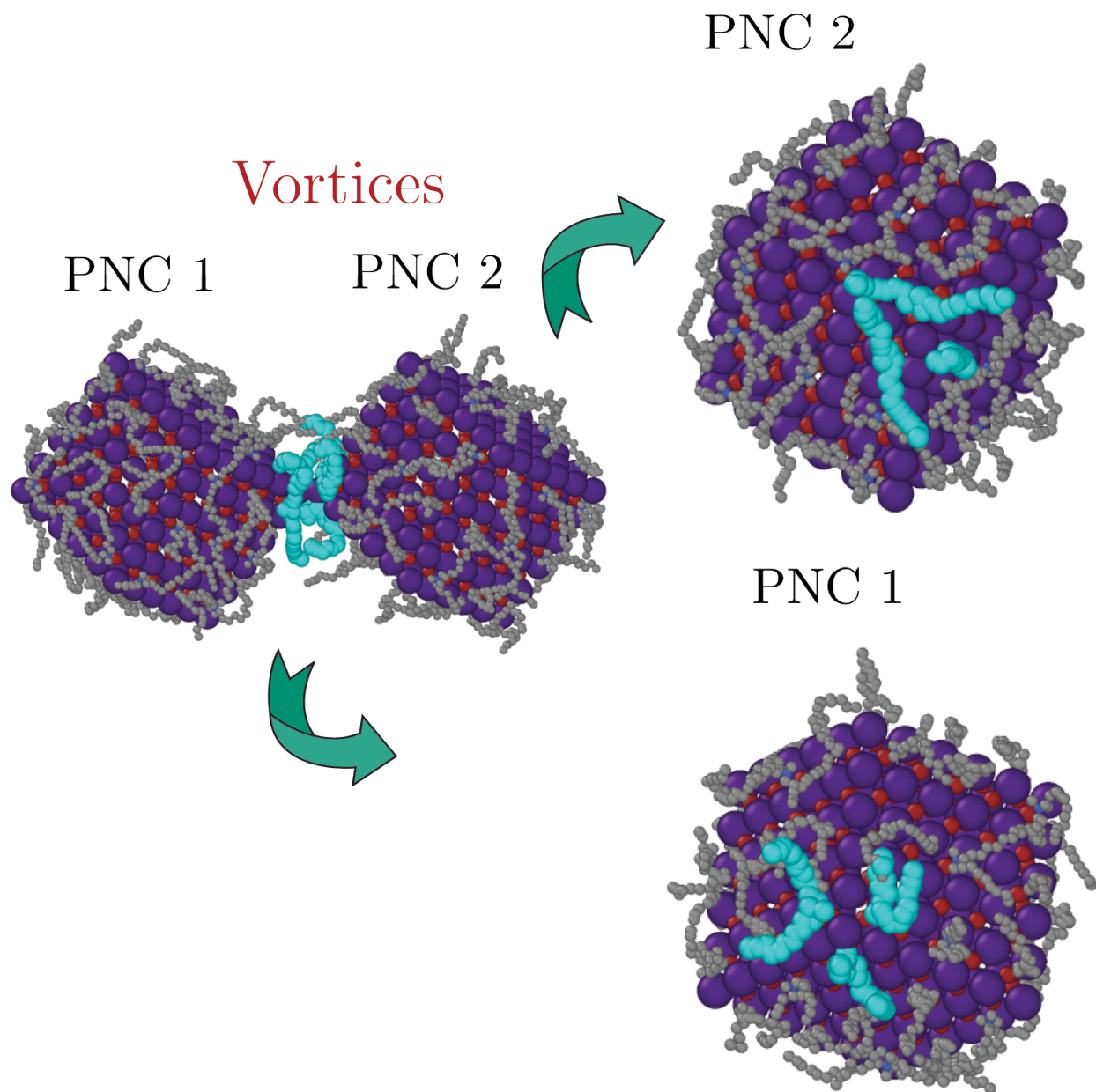


Figure S17: Vortices in corner-corner PMF, colored cyan.

References

- (1) Travesset, A. Soft Skyrmions, Spontaneous Valence and Selection Rules in Nanoparticle Superlattices. *ACS Nano* **2017**, *11*, 5375–5382.
- (2) Lai, K. C.; Zha, X.; Evans, J. W.; Travesset, A. Structure of Polydisperse fcc Nanocrystals: Implications for Crystal Fractionalization. *The Journal of Physical Chemistry C* **2019**, *123*, 9528–9537.
- (3) Bodnarchuk, M. I.; Boehme, S. C.; Ten Brinck, S.; Bernasconi, C.; Shynkarenko, Y.; Krieg, F.; Widmer, R.; Aeschlimann, B.; Günther, D.; Kovalenko, M. V.; Infante, I. Rationalizing and Controlling the Surface Structure and Electronic Passivation of Cesium Lead Halide Nanocrystals. *ACS Energy Letters* **2019**, *4*, 63–74.
- (4) Dong, Y.; Qiao, T.; Kim, D.; Parobek, D.; Rossi, D.; Son, D. H. Precise Control of Quantum Confinement in Cesium Lead Halide Perovskite Quantum Dots via Thermodynamic Equilibrium. *Nano Letters* **2018**, *18*, 3716–3722.
- (5) Boehme, S. C. et al. Strongly Confined CsPbBr₃ Quantum Dots as Quantum Emitters and Building Blocks for Rhombic Superlattices. *ACS Nano* **2023**, *17*, 2089–2100.
- (6) Cherniukh, I.; Rainò, G.; Stöferle, T.; Burian, M.; Travesset, A.; Naumenko, D.; Amenitsch, H.; Erni, R.; Mahrt, R. F.; Bodnarchuk, M. I.; Kovalenko, M. V. Perovskite-type superlattices from lead halide perovskite nanocubes. *Nature* **2021**, *593*, 535–542.
- (7) Waltmann, C.; Horst, N.; Travesset, A. Capping Ligand Vortices as "atomic Orbitals" in Nanocrystal Self-Assembly. *ACS Nano* **2017**, *11*, 11273–11282.